Biointerphases
a SpringerOpen Journal

ORIGINAL ARTICLE Open Access

Diatom attachment inhibition: limiting surface accessibility through air entrapment

Alex H-F Wu, Kenichi Nakanishi, KL Cho and Robert Lamb*

Abstract

Surfaces consisting of sub micron holes (0.420-0.765 μm) engineered into nanoparticle (12 nm) coatings were examined for marine antifouling behaviour that defines early stage settlement. Immersed surfaces were found to be resistant to a 5-hour attachment assay of *Amphora coffeaeformis*, a marine organism commonly found in abundance on fouled substrates such as foul-releasing paints and self-polishing coatings. Attachment inhibition was attributed to the accessibility of diatoms to the surface. This was governed by the size and morphology of trapped interfacial air pockets measured *in-situ* using synchrotron small angle x-ray scattering. Surfaces containing larger pores (0.765 μm) exhibited the highest resistance. Macroscopic wettability via contact angle measurements however remained at 160° and sliding angle of < 5° and was found to be independent of pore size and not indicative of early stage fouling behaviour. The balance of hierarchical nano/micro length scales was critical in defining the early stage stability of biofouling character of the interface.

Keywords: Superhydrophobic, Biofouling, Attachment-inhibition, Diatom, Amphora coffeaeformis, Air-entrapment

Background

Marine biofouling is the accumulation of marine species onto submerged surfaces within the ocean. It imposes significant cost to the maritime industries [1,2] and as a result has been the subject of a considerable number of preventative strategies. Until recently all of these have involved toxic coatings containing heavy metals such as copper and tin [3,4]. More recently, environmental considerations such as bioaccumulation [5,6] have led to the ban on many of these. This has resulted in a demand for non-toxic alternatives.

Current non-toxic antifouling strategies are driven by interfacial architecture and fall into two main behavioral categories, foul-release (FR) surfaces and attachment-inhibiting (AI) surfaces. FR surfaces seek to reduce the adhesion strength of attached organisms. This facilitates their removal [7-9] in dynamic situations, and thus is optimized for applications on moving vessels. In contrast, attachment-inhibiting (AI) surfaces rely on surface characteristics that completely deter initial attachment of marine organisms [10].

In both cases variations in chemistry and topography are the key features. Polyethylene glycol (PEG) is a good example of the former [11-13] while advances in analytical techniques such as electron microscopy has provided insights into naturally rough AI surfaces such as sharkskin and barnacle shells [9]. The apparent unique topography has fueled biomimetic designs for antifouling surfaces that exhibit antifouling properties [14,15]. In conjunction with this, several theories have been developed in order to explain the mechanism of action behind these types of AI surfaces [16-18]. All are focused on adsorption of organisms at the substrate/liquid interface. Attachment point theory describes the surface interactions in terms of the organisms' relative contact surface area [15,17,19] at the water/surface interface, where the size difference dictates adhesion strength. This has been demonstrated in individual species assays [14]. In practice however, the biofouling will eventually occur due to the range of organism sizes.

In contrast to fluid/surface interfaces, liquid/vapour interfaces do not attract adsorption of marine species irrespective of size. Superhydrophobic surfaces contain a blend of chemistry and topography that effectively traps air at the interface and leads to aqueous contact angles greater than 150°. The use of such surfaces for antifouling was first demonstrated experimentally by Zhang et al. [20]. They reported that while contact angle could

* Correspondence: rnlamb@unimelb.edu.au
School of Chemistry, University of Melbourne 3010, Melbourne, Australia

change it did not correlate necessarily with biofouling behaviour. In a more recent paper [13] it was shown that reduction in wetted area at the nanoscale was linked to biofouling behaviour. Changes in nanoscale wetting did not, however, impact markedly on the macroscopic contact angle value. Thus, creating surfaces that maintain trapped interfacial air may lead to a new class of antifouling coating.

In this work, the role of air in the attachment behaviour *Amphora coffeaeformis*, a commonly found organism on fouled surfaces [21-24], on superhydrophobic surfaces was investigated. *In-situ* synchrotron small angled x-ray scattering was used to examine the lower limits (nanoscale) of air entrapment on superhydrophobic surfaces with varying degrees of surface roughness, to elucidate whether the evolution of the air layer over time is the cause for differences in settlement of diatoms.

Methods

Synthesis of superhydrophobic coatings

Silica nanoparticles (Aerosil 200, av. dia. 12 nm, 0.25 g) was dispersed in ethanol (AR, 95%) by sonication (40 kHz, 10 min). Polymethylmethacrylate (PMMA) latex emulsion (av dia. 420 nm, 0.5 g) was added to the silica dispersion and further sonicated for 10 min. Methyltrimethoxysilane (MTMS) (98%, Sigma-Aldrich, 0.6 g) and concentrated HCl (36% w/v, AR, 60 μL) were added to the solution and allowed to react under sonication for 3 h to form the sol–gel solution [25].

This was repeated with various PMMA latex particle sizes: 485 nm, 572 nm, 635 nm, 671 nm, and 765 nm.

Synthesis of PMMA latex particles

PMMA latex particles were synthesized by charging a reaction vessel with ultrapure water (100 mL, Millipore), poly (dimethylsiloxane)-poly(ethylene oxide) block copolymer (5 g, Gelest, 400 cst, 25% non-siloxane), methylmethacrylate (10 g, Sigma-aldrich, 99%), Di(trimethylolpropane) tetraacrylate (1 g, Sigma-aldrich, 99%) and potassium persulfate (0.1 g, Sigma-aldrich, 99%). The mixture was vigorously mixed with mechanical stirring by a hand-held mixer (Braun Multiquick 300 Watts) for 5 minutes. It was then purged with Argon for 10 minutes under constant stirring with a magnetic stirrer set at 700 rpm. The mixture was then heated to 70-75°C for 3 hours with constant stirring. The ready emulsion was allowed to cool and filtered through cotton wool to remove coagulated PMMA.

Macroscopic wettability measurements of superhydrophobic surfaces

Each coating was subjected to contact angle measurements (Ramé-Hart Inc.) using the sessile drop method. The contact angle of each coating was measured at three different points to obtain a statistical average with reproducibility of ± 5°. Sliding angle was measured in triplicate by gradually tilting each surface by increments of 0.1 degrees, upon which a sessile drop of water is resting, until the water droplet rolls off the surface.

Inverse captive bubble measurements were conducted in a custom-built acrylic container filled with milli-Q water. Surfaces were immersed with the coated side facing down and a bubble (20 μL) was introduced into the chamber via a microsyringe with an inverted needle.

The surface coverage of air on immersed superhydrophobic surfaces was visually inspected by tiling an immersed surface 48° to a digital camera. This is the critical angle for total internal reflection at a water/air interface and is used to visualize changes in the coverage of air on surfaces before and after the attachment assay.

Nanoscopic wettability measurements using In-situ small-angle x-ray scattering (SAXS)

The amount of retained air on superhydrophobic surfaces after immersion in diatom culture media was quantified using transmission small-angle x-ray scattering measurements conducted at the Australian Synchrotron SAXS/WAXS beamline. All measurements were done with an x-ray wavelength of 1.512 Å with beam energy of 15 keV and a camera length set at 7 m. The scattering vector q has units of $Å^{-1}$ and is given by:

$$q = 4\pi \sin(\phi/2)\lambda \quad (1)$$

where ϕ is the scattering angle and λ is the irradiating wavelength.

Four custom-built fluid cells that allowed remote fluid injection through a peristaltic pump and a reservoir of filtered seawater water were used for the in-situ measurements. The cell was constructed from two sheets of 5 μm-thick kapton separated and sealed by a 1.4 mm-thick neoprene gasket. One of the kapton windows is coated experimentally. The cell could then be filled with fluid without changing its position relative to the incident x-ray beam. As the scan position and the physical morphology are not altered between scans, any change in scattering over time is attributed to a change in the nature of the interface between the coating and liquid.

Multiple SAXS measurements were made on different points on each sample, and the average is used as a representative SAXS profile for each sample. The x-ray beam irradiated a spot approximately 200 μm × 100 μm, with each sampling point spaced 500 μm apart. Ample distance between each measured point prevented overlap between irradiated points.

To measure the amount of entrapped air at the interface, SAXS measurements were first made on dry superhydrophobic surfaces. The fluid cell was then charged with the same diatom media that was used during the

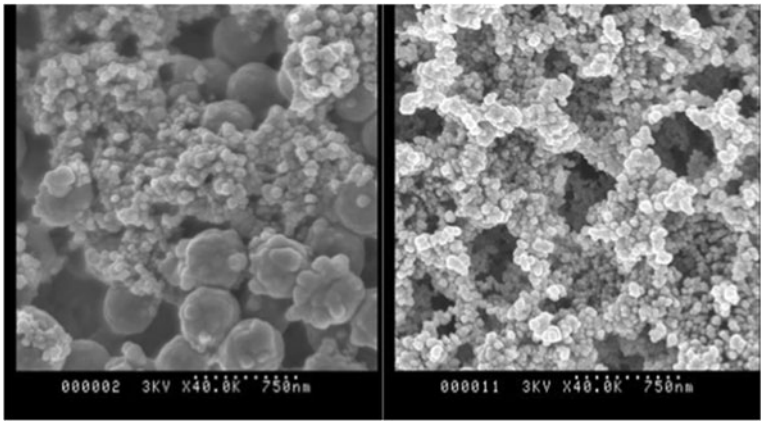

Figure 1 SEM micrograph of latex-templated superhydrophobic surface. Left) Before curing process, the presence of silica-encased PMMA spheres can be observed, and **Right)** The pores left behind after thermal decomposition of the PMMA latex.

attachment assay. This was prepared by culturing a batch of artificial seawater with the same concentration of diatoms as those used in the attachment assay for 5 hours. The mixture was then centrifuged and the supernatant was collected. This minimized the likelihood of diatoms contributing to the x-ray scattering profile, as well as to simulate the maximum possible amount of extracellular polymeric substances (EPS) available within the media during the nanowetting study.

This diatom culture media was then introduced into the fluid cell, and SAXS measurements were made at each point every 10 minutes up to 360 minutes, which corresponds to the length of time required for a diatom attachment assay. To obtain a SAXS profile of immersed superhydrophobic surfaces in the fully wetted regime, the fluid within the cell was exchanged with ethanol, followed by water. The ethanol was used as a wetting agent, to remove air from the interface and thereby forcing the immersed superhydrophobic surfaces into a wetted Wenzel state when water was reintroduced.

Species attachment assays – diatoms (amphora coffeaeformis)

Coated glass slides were placed in culture wells with a maximum volume capacity of 40 mL. Diatoms ($\phi \sim 16$ μm) were cultured in K+ media for at least 48 hours under a 12-hour day/night cycle under controlled temperature and humidity in a culture fridge. The diatoms were concentrated by centrifugation and the number of diatoms/mL was counted using a haemocytometer. Each well was charged with 20 mL of artificial seawater pre-dispersed with 1 mL of concentrated diatom culture, and the number of diatoms per well is normalized against the haemocytometer count. The immersed surfaces were then left in the culture fridge for 5 hours and were then immersed in 10 L of artificial seawater to dislodge any unsettled diatoms. Care was exercised to keep all surfaces immersed in artificial seawater to prevent disrupting settled diatoms due to dewetting mechanisms.

Settlement of diatoms was characterized using fluorescence microscopy on a Leica DM2500 confocal fluorescence microscope coupled to a Leica DC300F camera. Images produces were 1300 x 1030 pixels. A 5x magnification lens was used to give a field of view (FOV) roughly equal to 17.4 mm^2. A mercury arc lamp using a Leica I3

Table 1 Wetting characteristics of superhydrophobic surfaces

Surface (Pore size)	Static contact angle (θ)	Sliding angle (θ)
A (420 nm)	166 ± 5	4 ± 2
B (485 nm)	162 ± 5	5 ± 2
C (572 nm)	160 ± 5	4 ± 2
D (635 nm)	164 ± 5	4 ± 2
E (671 nm)	164 ± 5	3 ± 2
F (765 nm)	166 ± 5	2 ± 2

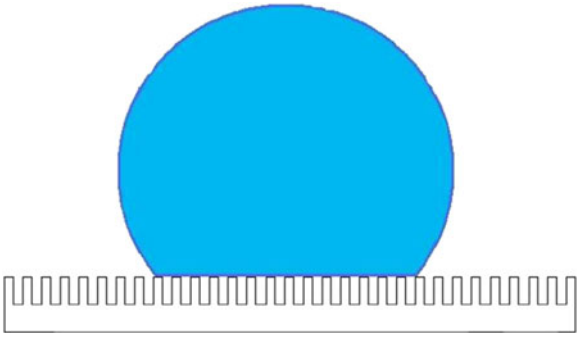

Figure 2 Schematic of a droplet sitting on a surface in the Cassie regime.

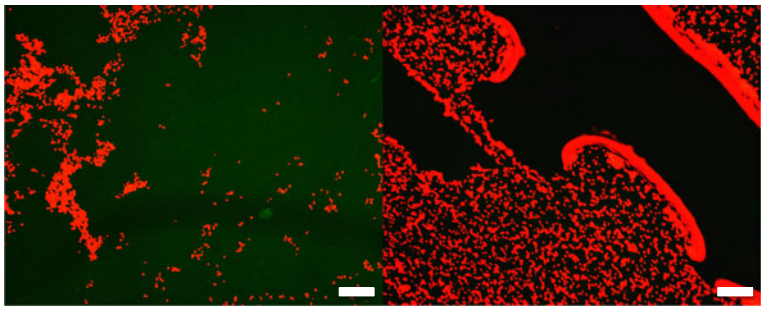

Figure 3 In-situ fluorescence microscope image of superhydrophobic surfaces after 5-hour diatom settlement assay. Left) Image taken without visible bubbles in FOV and, **Right)** A tubular bubble can be seen running diagonally through the FOV. The lens effect can be seen clearly where the fluorescence of diatoms are close to the bubble edge. (Scale bar: 150 μm).

filter cube (blue excitation 450–490 nm) enabled the chlorophyll in *Amphora coffeaeformis* to fluoresce a very strong shade red. Images were captured on 10 random FOVs per surface using Leica's camera software, IM50, with the bright field (BF) setting in place. Image analysis was conducted using Adobe Photoshop Elements 2.0, 2002, with a colour tolerance figure of 200 to maximize the fluorescence intensity. This allowed for automatic quantification of red pixels against a dark background.

Results

Surface properties

All surfaces were fabricated by aggregating silica nanoparticles in a hydrophobic gel around PMMA latex particles, which were removed thermally during the curing process, leaving behind pores [25]. The resulting structure resembles a honeycomb constructed using nanoparticles (Figure 1).

Further details and structural characterization of these surfaces can be found elsewhere [25]. The pore size was varied by incorporating latex particles of different sizes during the sol–gel reaction, which were then thermally removed. The latex particles were synthesized using a method described elsewhere [26], and ranged from 400 nm to 765 nm in diameter. The size range chosen was at least an order of magnitude smaller than the size of marine organisms used in this study to circumvent the effects of attachment point theory.

The fabricated surfaces were superhydrophobic in nature with high contact angles (> 160°) and low sliding angles (< 5°) (Table 1).

The contact angle on a superhydrophobic surface can be expressed by the Cassie and Baxter equation by postulating that the measured contact angle is in fact a summation of N surface chemical species, as expressed in equation 2 [27].

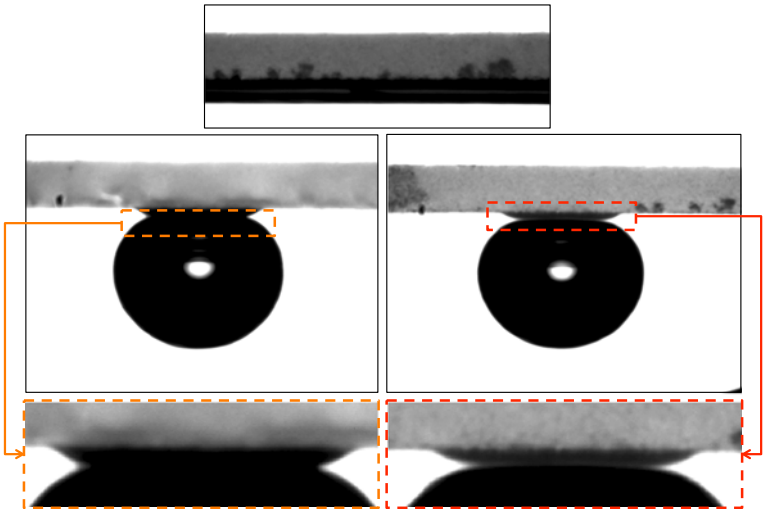

Figure 4 Inverse captive bubble images of Top) Superhydrophobic surface, where the black band is indicative of a smooth layer of air at the interface, Left) Glass substrate, Right) Superhydrophobic surface after ethanol treatment and water flushing.

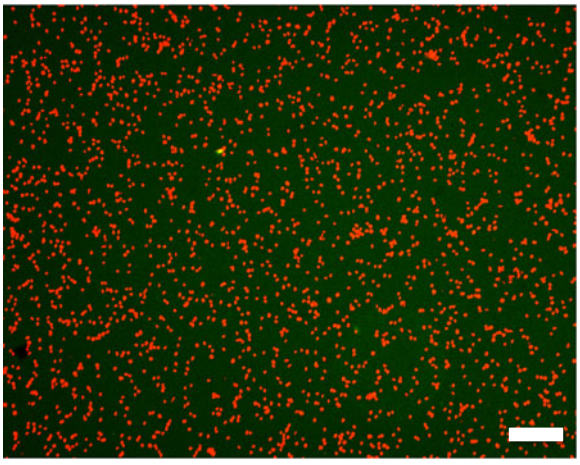

Figure 5 In-situ fluorescence microscope image of a superhydrophobic surface after a 5-hour diatom settlement assay. Uniform distribution of diatoms can be seen with little clustering observed. (Scale bar: 150 μm).

$$\cos\theta^{*}_{CA} = \frac{1}{\gamma_{LG}} \sum_{n=1}^{N} f_n \left(\gamma_{n,SG} - \gamma_{n,SL} \right), \quad where \quad \sum_{n=1}^{N} f_n = 1 \tag{2}$$

Where f_n is the fractional coverage of the n^{th} chemical specie with interfacial energies $\gamma_{n,\,SG}$ and $\gamma_{n,\,SL}$. Consider a two-component surface, where one component is a hydrophobic substrate, and the other is air, as illustrated in Figure 2. This results in a Cassie regime, where air pockets are trapped between the water/surface interface.

Effect of Air on attachment behaviour of Amphora coffeaeformis

Fluorescence microscopy was used to characterize the extent of which diatoms were attached onto each superhydrophobic surface. Prior to imaging, each of the surfaces were immersed in fresh filtered seawater and gently perturbed to remove any free-flowing and weakly attached diatoms. Due to the presence of shearing forces at the fluid/air/surface interface that may dislodge bound diatoms during dewetting phenomena, extra care was exercised to ensure none of the surfaces were re-exposed to air until after fluorescence microscope images were taken.

Fluorescence microscopy images were taken *in-situ* at regions with and without visible air pockets. In regions where the air pocket size was larger than the field-of-view (FOV) of the microscope, no diatoms were found. In regions without air pockets, or with air pockets small enough to elude the naked eye, large colonies of diatoms were observed (Figure 3).

To ascertain the effect of air on the settlement behaviour of diatoms, the assay was repeated on superhydrophobic surfaces after an ethanol wetting treatment as described in the methods section. The ethanol introduced initially was continuously washed out with milliQ water until the surface tension of the effluent returned to that of pure water (72.8 mN/m @ 25°C), at which point, a further 10 dilutions were performed to ensure minimal residual ethanol remained (henceforth referred to as wetted surfaces). To confirm the total removal of entrapped air on immersed superhydrophobic surfaces, the contact angle of an inverse captive bubble under water was measured, which was found to be similar to that of a cleaned glass substrate (Figure 4). Furthermore,

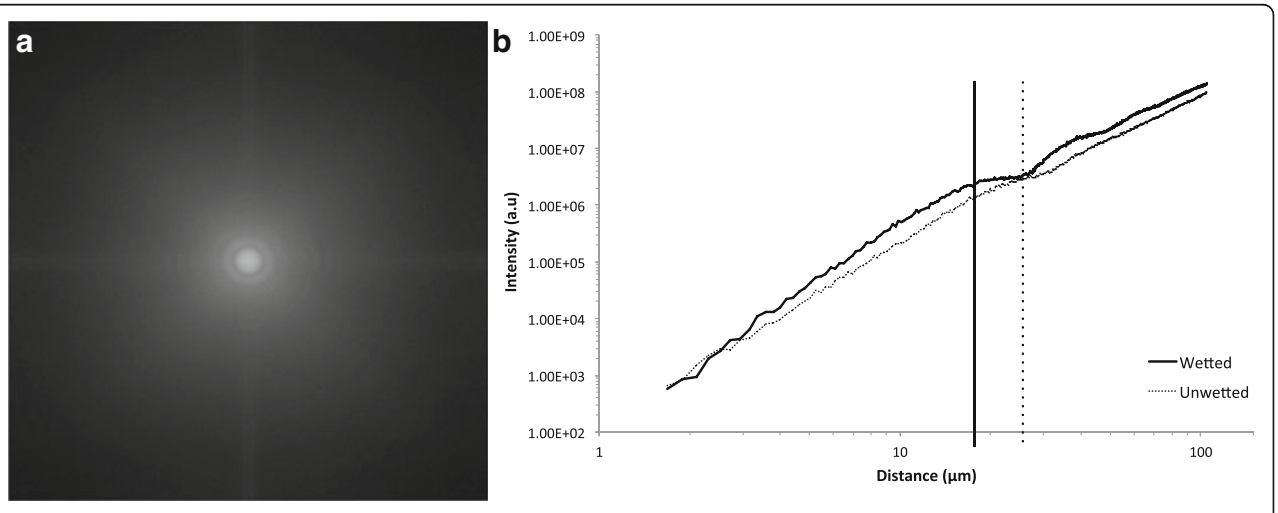

Figure 6 a) 2D FT power spectrum of the fluorescence image. b) Intensity of the power spectrum averaged across the same frequency fringe. Solid Line: Wetted superhydrophobic surface; Dashed line: Unwetted superhydrophobic surface.

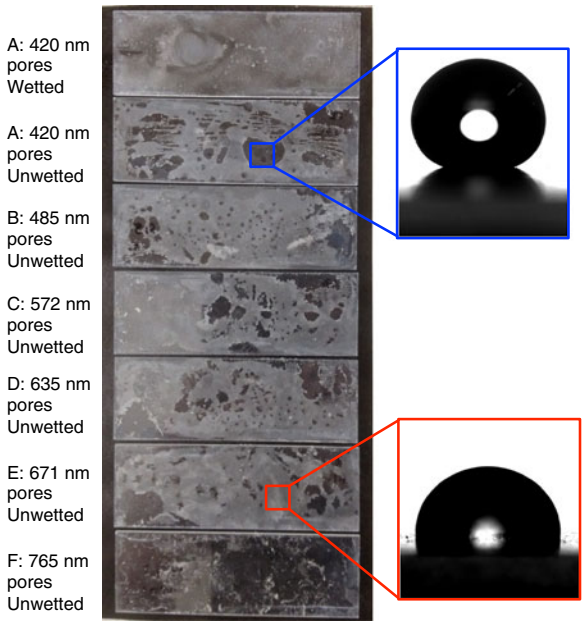

Figure 7 Image of superhydrophobic surfaces dried after 5-hour diatom settlement assay. The surfaces are transparent in nature and are placed on a black surface for clarity. Dark regions indicate the presence of bubbles remaining after 5 hours of immersion, whereas opaque regions are fouled. This was confirmed with contact angle measurements where the ability for the surface to retain air is lost after fouling.

a 'gap' was observed to be present between the wetted superhydrophobic substrate and the captive bubble, which is indicated by a band of light transmitting through the bubble/surface interface, indicating that a thin layer of water is present at the bubble/surface interface. This confirms that the surface has been completely wetted and that no air pockets remain at the surface.

Fluorescence microscopy images of the wetted superhydrophobic surfaces were taken *in-situ* after the 5-hour diatom settlement assay (Figure 5). Diatoms were distributed on the surface uniformly with little evidence of clustering, as seen in Figure 3.

To clarify differences in diatom settlement behaviour between wetted and un-wetted surfaces, a 2D Fourier transform (FT) image analysis was performed on all fluorescence microscopy images. Fourier analysis is a powerful tool for image analysis and can be used to elucidate the size and spacing between features. Figure 6a shows the power spectrum of an *in-situ* fluorescence microscope image of a superhydrophobic surface after the 5-hour diatom assay (Figure 6a) calculated using 2D FT. The intensity of concentric fringes of the power spectrum was then averaged to yield a plot of intensity versus spatial frequency, which is used to elucidate mean feature sizes and inter-feature distance (Figure 6b).

Two distinct features can be observed in the averaged power spectrum plots of all wetted superhydrophobic surfaces (Figure 6b); a prominent peak at approximately 17 μm, representing the size of diatoms, and a decaying oscillation that represents the periodicity of diatom distribution in all directions. This indicates that all settled diatoms are roughly equidistant to one another on the wetted superhydrophobic surface, an observation similar to those of smooth surfaces.

While a similar peak was also observed for fluorescent images of unwetted superhydrophobic surfaces, this peak appeared at around 26 μm, indicating that the diatoms are clustered in pairs or more. Furthermore, the decaying oscillation was not observed. This is because diatoms are no longer evenly distributed on the surface, but rather, exhibit signs of clustering.

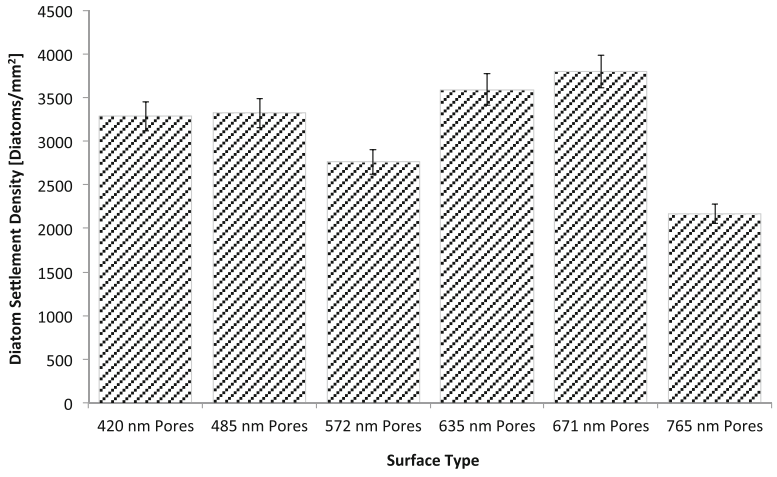

Figure 8 Density of diatom settlement as a function of pores size of superhydrophobic surfaces.

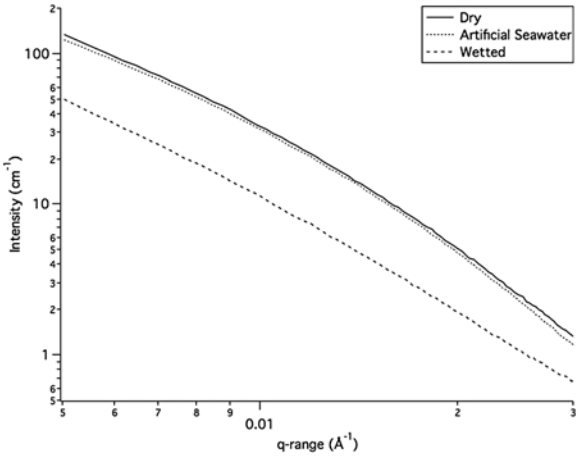

Figure 9 Synchrotron in-situ SAXS profile for superhydrophobic surfaces under dry conditions, immersion in artificial seawater, and completely wetted. Note that the degree of wetting is proportional to the intensity drop of the scattering profile.

Effect of surface morphology on attachment behaviour of Amphora coffeaeformis

The wettability of all superhydrophobic surfaces was visibly different after a 5-hour immersion in artificial seawater during the diatom species assay. Initially, a reflection at the surface/fluid interface was found at a glancing angle of approximately 48° when the surfaces were immersed. This was almost identical to the reflection at a fluid/air boundary, which suggests that a uniform layer of air resides at the fluid/surface interface of immersed superhydrophobic surfaces. Over the 5-hour assay, emergence of air pockets with a visibly large radius of curvature was observed on all surfaces, and the reflection was no longer uniformly distributed across the entire sample. This suggests that during the assay, localised wetting has occurred, resulting in the partial loss of the glancing reflection at the interface.

The effect of pore size on diatom settlement behaviour was apparent when the superhydrophobic surfaces were removed from the fouling media and left to dry overnight. After drying, a mixture of diatoms, protein/enzyme biofilm and salt crystals formed an opaque film on the superhydrophobic surfaces. The fractional coverage of this opaque film over each surface decreased with increasing pore size, suggesting that superhydrophobic surfaces constructed with larger pore size resisted wetting phenomena, whereby a large proportion of the surface retained an air layer that maintained a pristine surface. This was confirmed when a series of contact angle measurements were made on different regions of each surface (Figure 7). It was evident that regions where air pockets remained after the 5-hour immersion maintained its superhydrophobic characteristics, whereas the contact angle of wetted and fouled regions decreased significantly.

Figure 8 shows the density of diatoms settled in regions where air pockets were minimal or absent on different surfaces. Within statistical significance, the density of settled diatoms between each superhydrophobic surface was consistent, suggesting that diatoms settlement behaviour is only influenced by the presence of air, not the underlying variations in surface roughness.

Quantification of trapped air using in-situ synchrotron transmission SAXS

Transmission SAXS measurements based on the technique described previously [28,29] were used to measure the immersed superhydrophobic surfaces over a scattering q-range of $0.003 < q < 0.1$, where the scattering momentum q is a function of the x-ray scattering angle ϕ and x-ray wavelength λ, given by equation (1). To avoid

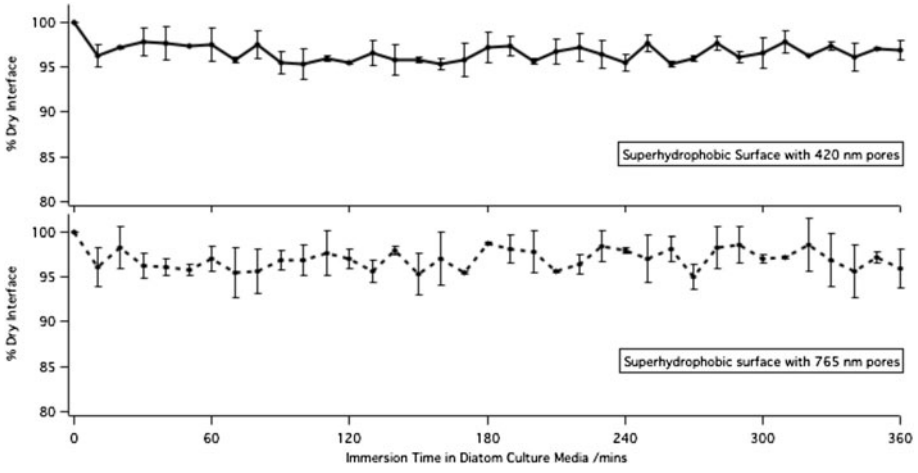

Figure 10 Percentage interface that remains dry on superhydrophobic surfaces immersed in diatom culture media as a function of time measured using in-situ small-angle x-ray scattering.

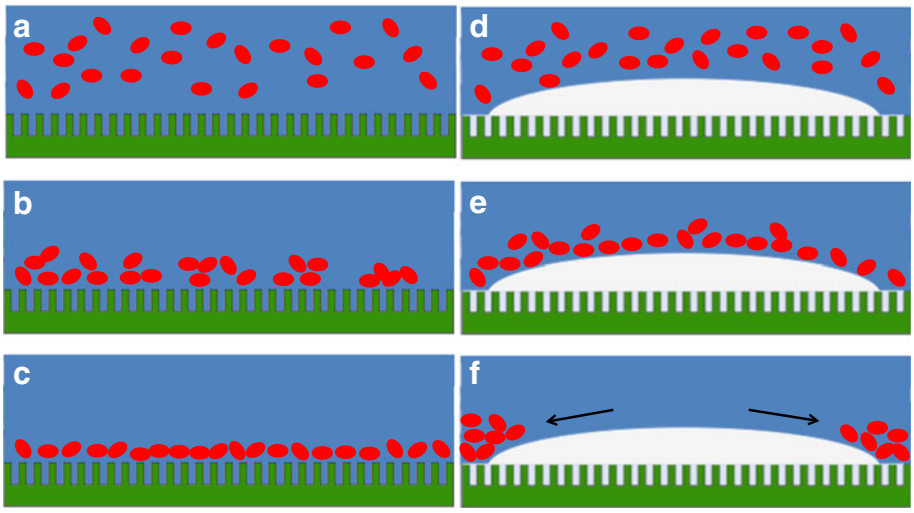

Figure 11 Schematic demonstrating the effect of air at the surface/fluid interface on settlement of diatoms. Figures **a)** – **c)** represents a surface without entrapped air pockets, **d)** – **f)** represents a surface with entrapped air.

effects of fluid compressibility at high q and resolution limit at extremely low q, the data analysis range was narrowed to between $0.005 < q < 0.03$.

The intensity I_{AB} of x-ray scattering into a given solid angle from a rough interface between two media with average electron densities ρ_A and ρ_B is proportional to the square of the difference between the densities. This results in high scattering intensity at interfaces with a large electron density difference. So with a dry superhydrophobic surface, x-ray scattering arises from the electron density difference between air and the surface. It has been shown previously that as wetting progresses on an immersed superhydrophobic surface, x-ray scattering intensity decreases as the air/surface interface is replaced by a water/surface interface [28].

In all immersed superhydrophobic surfaces, the scattering profile at high q can be described using the Porod slope:

$$I(q) = Bq^{-4} \tag{3}$$

This equation holds a special significance when the exponent of q is equal to −4, which is the case for all measured surfaces in this study. The pre-factor B is directly proportional to the total amount of interface that is illuminated by the x-ray beam. As air/surface interface is replaced with water/surface interface during wetting, the pre-factor B can be used to directly quantify the percentage of surface that remains dry [28].

In the case of the surface/air/water interface of immersed superhydrophobic surfaces, the SAXS profile of a wetted substratum is lower in scattering intensity than a dry substratum, as shown in Figure 9.

The SAXS profiles obtained suggest that superhydrophobic surfaces immersed in artificial seawater exhibited a degree of resilience against wetting as the surface virtually remains dry after initial immersion. Figure 10 also shows the percentage dry interface remaining on an immersed superhydrophobic surface as a function of time. The per-

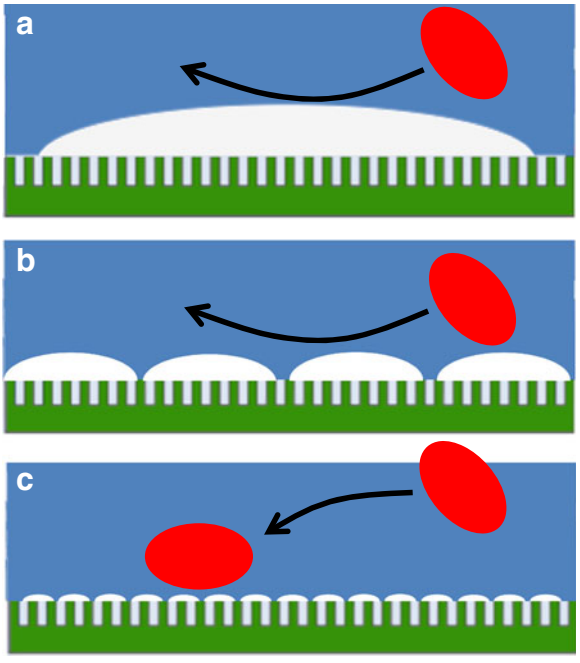

Figure 12 Schematic demonstrating the effect of air pocket size on attachment of diatoms. Attachment is inhibited when **a**) Air pocket size > diatom and **b**) when size of air pocket ~ diatom, but attachment is not inhibited **c**) when size of air pocket < diatom.

pre-factor B at time t by the pre-factor B when the interface is completely dry.

$$\%\ \text{dry interface} = B_t/B_{dry} \quad (4)$$

Figure 10 shows the % dry interface on superhydrophobic surfaces immersed in diatom culture media over 6 hours. It can be seen that during the wetting study, the percentage surface that remains dry is consistent, suggesting that no further wetting has progressed for both superhydrophobic surfaces.

Discussion

Effect of air pockets on attachment of Amphora coffeaeformis

From the attachment assays, it can be seen that the air at the interface of immersed superhydrophobic surfaces prevent attachment of *Amphora coffeaeformis*. This agrees with the theory proposed by Zhang et al. [20] whereby a reduction in contact surface area between fluid and surface will induce a reduction in attachment probability of marine organisms. This was further supported by the Fourier transform analysis conducted on each fluorescent image, whereupon the power spectrum highlights the presence of clustering of diatoms around the edges of the air pockets (Figure 6).

Clustering is a natural outcome of the diatoms settling mechanism in which they are passive settlers until they reach a surface. Fluorescence images suggest that diatoms are driven away from air pockets through either their gliding mechanism, or a consequence of gravity. This means that while diatoms can drift onto existing entrapped air pockets or the surface indiscriminately, upon landing, diatoms will be driven towards a more favourable settling position, resulting in the observed clustering of diatoms in fluorescent images of un-wetted superhydrophobic surfaces (Figure 11).

Effect of surface morphology on attachment of Amphora coffeaeformis

It is worth noting that while diatom attachment is reduced significantly on surfaces fabricated using larger pores (Figure 7), on areas where air pockets are absent, the number of diatoms as measured by the % coverage of red pixels, is statistically consistent across all superhydrophobic surfaces (Figure 8). Considering that the fluid/surface interface at the nanoscale remained consistent throughout the diatom assay, and that the contact angle has dropped only on surfaces with smaller pores, this suggests that the settlement of diatoms on superhydrophobic surfaces was significantly inhibited by the presence of larger air pockets, not nanoscopic ones.

A schematic demonstrating this effect is shown in Figure 12. Akin to attachment point theory, the presence of air pockets reduces the contact point of diatoms onto superhydrophobic surfaces.

The difference resides in the fact while the size of air pockets are large initially on all superhydrophobic surfaces, which gives rise to the high water contact angles, the stability of these larger air pockets can be fine-tuned by surface roughness. According to this theory, it seems to suggest that the significant variation in surface coverage by biofilms between surfaces with different pore sizes can be attributed to the relative stability of larger air pockets retained on the surface. While the mechanism behind this difference is still under investigation, the presence of air pockets and its morphology has a significant influence over the settlement behaviour of *Amphora coffeaeformis*.

Conclusion

The presence of air is a physical barrier against organism attachment due to reduced fluid/surface contact area. The presence of air at the surface/liquid interface limits the accessibility of diatoms (*Amphora coffeaeformis*) to the surfaces, thus reducing settlement probability. Through attachment assays of diatoms and direct measurement of the water/air/surface interface of an immersed superhydrophobic surface using in-situ small-angle x-ray scattering, it was found diatom attachment was inhibited on macroscopic air pockets, but not nanoscopic ones. This suggests that the attachment-inhibiting characteristics of superhydrophobic surfaces may depend on the size of the air pockets present on immersed superhydrophobic surfaces rather than a simple measure of surface wettability.

Competing interests

The authors declare that they have no competing interests.

Authors' contributions

AW carried out the synchrotron SAXS experiments and subsequent data analysis, and Fourier transform image analysis. KN fabricated all superhydrophobic coatings and conducted diatom attachment assays. KC assisted in the SAXS experiments. All authors contributed equally to the drafting of the manuscript. All authors read and approved the final manuscript.

Received: 28 August 2012 Accepted: 7 January 2013
Published: 7 February 2013

References

1. Schultz MP (2007) Effects of coating roughness and biofouling on ship resistance and powering. Biofouling 23(5):331–341. doi:10.1080/08927010701461974
2. Schultz MP, Bendick JA, Holm ER, Hertel WM (2011) Economic impact of biofouling on a naval surface ship. Biofouling 27(1):87–98. doi:10.1080/08927014.2010.542809
3. Willemsen PR, Ferrari GM (1993) The use of anti-fouling compounds from sponges in anti-fouling paints. Surface Coatings International 76(10):423–427
4. Suzuki T, Matsuda R, Saito Y (1992) Molecular species of tri-n-butyltin compounds in marine products. J Agric Food Chem 40(8):1437–1443. doi:10.1021/jf00020a030
5. Champ MA (2000) A review of organotin regulatory strategies, pending actions, related costs and benefits. Sci Total Environ 258(1–2):21–71
6. Abbott A, Abel PD, Arnold DW, Milne A (2000) Cost-benefit analysis of the use of TBT: the case for a treatment approach. Sci Total Environ 258(1–2):5–19

7. Callow JA, Callow ME (2011) Trends in the development of environmentally friendly fouling-resistant marine coatings. Nat Commun 2:244
8. Banerjee I, Pangule RC, Kane RS (2011) Antifouling coatings: recent developments in the design of surfaces that prevent fouling by proteins, bacteria, and marine organisms. Adv Mater 23(6):690–718. doi:10.1002/adma.201001215
9. Scardino AJ, de Nys R (2011) Mini review: biomimetic models and bioinspired surfaces for fouling control. Biofouling 27(1):73–86. doi:10.1080/08927014.2010.536837
10. Cao X, Pettitt ME, Wode F, Arpa Sancet MP, Fu J, Ji J, Callow ME, Callow JA, Rosenhahn A, Grunze M (2010) Interaction of zoospores of the green alga ulva with bioinspired micro- and nanostructured surfaces prepared by polyelectrolyte layer-by-layer self-assembly. Adv Funct Mater 20(12):1984–1993. doi:10.1002/adfm.201000242
11. Magin CM, Finlay JA, Clay G, Callow ME, Callow JA, Brennan AB (2011) Antifouling performance of cross-linked hydrogels: refinement of an attachment model. Biomacromolecules 12(4):915–922. doi:10.1021/bm101229v
12. Ekblad T, Bergström G, Ederth T, Conlan SL, Mutton R, Clare AS, Wang S, Liu Y, Zhao Q, D' Souza F, Donnelly GT, Willemsen PR, Pettitt ME, Callow ME, Callow JA, Liedberg B (2008) Poly(ethylene glycol)-containing hydrogel surfaces for antifouling applications in marine and freshwater environments. Biomacromolecules 9(10):2775–2783. doi:10.1021/bm800547m
13. Rosenhahn A, Schilp S, Kreuzer HJ, Grunze M (2010) The role of "inert" surface chemistry in marine biofouling prevention. Phys Chem Chem Phys 12(17):4275–4286
14. Schumacher J, Carman M, Estes T, Feinberg A, Wilson L, Callow M, Callow J, Finlay J, Brennan A (2007) Engineered antifouling microtopographies - effect of feature size, geometry, and roughness on settlement of zoospores of the green alga Ulva. Biofouling 23(1):55–62
15. Callow ME, Jennings AR, Brennan AB, Seegert CE, Gibson A, Wilson L, Feinberg A, Baney R, Callow JA (2002) Microtopographic cues for settlement of zoospores of the green fouling alga enteromorpha. Biofouling 18(3):229–236
16. Scardino AJ, Zhang H, Lamb RN, Cookson DJ, Rd N (2009) The role of nano-roughness in antifouling. Biofouling 25(8):757–767
17. Scardino AJ, Harvey E, De Nys R (2006) Testing attachment point theory: diatom attachment on microtextured polyimide biomimics. Biofouling 22 (1):55–60
18. Schumacher JF, Long CJ, Callow ME, Finlay JA, Callow JA, Brennan AB (2008) Engineered nanoforce gradients for inhibition of settlement (attachment) of swimming algal spores. Langmuir 24(9):4931–4937. doi:10.1021/la703421v
19. Scardino AJ, Guenther J, de Nys R (2008) Attachment point theory revisited: the fouling response to a microtextured matrix. Biofouling 24(1):45–53
20. Zhang H, Lamb R, Lewis J (2005) Engineering nanoscale roughness on hydrophobic surface-preliminary assessment of fouling behaviour. Sci Technol Adv Mater 6(3–4):236–239
21. Callow (1986) A world-wide survey of slime formation in antifouling paints. In: Evans LV, Hoagland KD (eds) Algal biofouling. Elsevier Science Publishers.1, Amsterdam (the Netherlands)
22. Cassé F, Swain GW (2006) The development of microfouling on four commercial antifouling coatings under static and dynamic immersion. International Biodeterioration and Biodegradation 57(3):179–185. doi:10.1016/j.ibiod.2006.02.008
23. Molino PJ, Campbell E, Wetherbee R (2009) Development of the initial diatom microfouling layer on antifouling and fouling-release surfaces in temperate and tropical Australia. Biofouling 25(8):685–694
24. Zargiel KA, Coogan JS, Swain GW (2011) Diatom community structure on commercially available ship hull coatings. Biofouling 27(9):955–965. doi:10.1080/08927014.2011.618268
25. Cho KL, Wu AHF, Lamb RN, Liaw II (2010) Influence of roughness on a transparent superhydrophobic coating. J Phys Chem C 114(25):11228–11233. doi:10.1021/jp103479k
26. Wu AHF, Cho KL, Liaw II, Zhang H, Lamb RN (2009) Synthesis of Poly (Methylmethacrylate) Latex With Enhanced Rigidity Through Surfactant Control. In: Bauer S, Cheng Z, Wrobleski DA, Zhang Q (eds) Polymer-Based Smart Materials - Processes, Properties and Application, vol 1134. Materials Research Society Symposium Proceedings., pp 109–114
27. Cassie ABD, Baxter S (1945) Large contact angles of plant and animal surfaces. Nature 155:21–22
28. Zhang H, Lamb RN, Cookson DJ (2007) Nanowetting of rough superhydrophobic surfaces. Appl Phys Lett 91, Art. no. 254106
29. Scardino AJ, Zhang H, Cookson DJ, Lamb RN, de Nys R (2009) The role of nano-roughness in antifouling. Biofouling 25(8):757–767

doi:10.1186/1559-4106-8-5
Cite this article as: Wu *et al.*: Diatom attachment inhibition: limiting surface accessibility through air entrapment. *Biointerphases* 2013 **8**:5.